Reflective semiconductor optical amplifiers-based all-optical NOR and XNOR logic gates at 120 Gb/s

Amer Kotb & Chunlei Guo

Published online: 22 Dec 2020.

Submit your article to this journal ⎘

Article views: 50

View related articles ⎘

View Crossmark data ⎘

Check for updates

Reflective semiconductor optical amplifiers-based all-optical NOR and XNOR logic gates at 120 Gb/s

Amer Kotb [a,b] and Chunlei Guo [c]

aThe GPL Photonics Laboratory, Changchun Institute of Optics, Fine Mechanics, and Physics, Chinese Academy of Sciences, Changchun, People's Republic of China; bDepartment of Physics, Faculty of Science, University of Fayoum, Fayoum, Egypt; cThe Institute of Optics, University of Rochester, Rochester, New York, USA

ABSTRACT

In this paper, we reported a reflective semiconductor optical amplifier (RSOA), in which the input light propagates and reflects back to the input port after amplifying twice through its active region. The RSOA produces higher gain and lower noise figure at low drive currents with energy-efficient than the conventional SOAs. The RSOA's features are employed herein to numerically analyze the ultrafast performance of the all-optical NOT-OR (NOR) and Exclusive-NOR (XNOR) logic gates using a dual-RSOAs-based scheme at 120 Gb/s. A comparison between RSOAs- and conventional SOAs-based AO NOR and XNOR gates is made by studying the quality factor (QF) against the critical operational parameters when the effects of the amplified spontaneous emission and the operating temperature are included to obtain more realistic results. Compared to conventional SOAs, the RSOAs allow to achieve more acceptable performance at 120 Gb/s and to render the implementation of the NOR and XNOR gates more feasible.

1. Introduction

So far the performance of the all-optical (AO) NOT-OR (NOR) and Exclusive-NOR (XNOR) logic gates have been investigated using semiconductor optical amplifiers (SOAs) at different data rates [1–22]. However, the SOA as a single-pass amplifier has very low reflectivity coatings on both facets whose gain saturates monotonically along its length [23]. However, the signal processing applications do not exceed ~ 100 Gb/s due to the slow gain and phase dynamics of the SOAs [24] and hence cannot upgrade to the sub-Tb/s region and beyond [25,26]. On the other hand, a reflective semiconductor optical amplifier (RSOA) has a similar waveguide structure to conventional SOA but with higher optical gain and lower noise figure at low drive currents with energy-efficient [24]. RSOA has an anti-reflective (AR) coating on its front facet, which is used as input and output ports, and a high-reflectivity (HR) coating on the rear facet. The schematic of the RSOA is illustrated in Figure 1 [27,28]. Because of the RSOA's construction, the input light is amplified and reflected back to the front port, from which the signal enters the RSOA, after passing twice through the RSOA's active region. This feedback process due to

the forward and backward travelling waves in the RSOA active region causes a strong gain saturation at low input power [23]. The RSOAs have been fabricated to operate at 1550 and 1300 nm wavelengths [24]. Owing to the RSOAs' characteristics, RSOAs have the potential for realizing the Boolean functions with obviating the need for extra optical fibre components and multiple optoelectronics optical devices. In this context, It would further be interested to employ the RSOA to investigate the AO NOR and XNOR logic gates. Unlike previous thankful efforts [1–22], this is done at a data rate of 120 Gb/s using dual-RSOAs-based schemes. For your information, the logic gates, XOR [27] and NAND [28], were implemented using the RSOA technology at 120 GB/s, but the gates NOR and XNOR were not implemented. Therefore, in this research, we complete and extend our previous work [27,28] by studying these two gates based on the RSOAs at 120 Gb/s. This is done through examining the dependence of the gates' quality factor (QF) on the critical operational parameters such as rear-facet reflectivity (R), internal loss coefficient, operating data rate, and pseudorandom binary sequence (PRBS), considering the effects of the amplified spontaneous emission (ASE)

CONTACT Amer Kotb ✉ amer@ciomp.ac.cn 🖳 The GPL Photonics Laboratory, Changchun Institute of Optics, Fine Mechanics, and Physics, Chinese Academy of Sciences, 130033, Changchun, People's Republic of China; Department of Physics, Faculty of Science, University of Fayoum, 63514, Fayoum, Egypt; Chunlei Guo ✉ guo@optics.rochester.edu The Institute of Optics, University of Rochester, 14627, Rochester, New York, USA
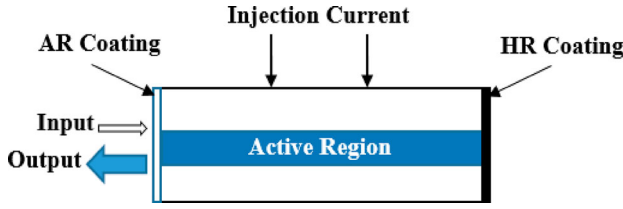
Figure 1. Schematic of RSOA.

and the operating temperature for more realistic calculations. To prove the preference of the RSOA, we put it in a fair comparison with conventional bulk SOA. The outcomes confirm that the AO NOR and XNOR logic gates can be realized using RSOAs at 120 Gb/s with higher QF than conventional SOAs.

The rest of this article is organized as follows: Section 2 describes the RSOAs numerical analysis. This is followed by NOR and XNOR gates in Sections 3 and 4, respectively. Finally, Section 5 concludes the obtained results.

Numerical analysis

The numerical analysis of RSOAs is a helpful means for theoretically describing, predicting, and optimizing their behaviour. The RSOA operation is theoretically analyzed based on the computationally accurate models mentioned in Refs. [29–34], which analytically involve solving a set of coupled partial nonlinear differential equations, including the nonlinear effects of interband and intraband. The intraband effects of the carrier heating (CH) and the spectral hole burning (SHB) occur in a time not exceeding a few picoseconds and have earning contributions in the optical gain that cannot be ignored. Considering the nonlinear interband effect of the carrier depletion (CD) and the intraband nonlinear effects of the CH and the SHB, the time-dependent gain of each RSOA is described by the following first-order differential equations [27,28]:

$$\frac{dh_{CD}(t)}{dt} = \frac{h_0 - h_{CD}(t)}{\tau_C} - \frac{h_{CD}(t)}{h_{CD}(t) - \alpha_{loss}L}$$
$$\times (\exp[h_{CD}(t) + h_{CH}(t) + h_{SHB}(t)$$
$$- \alpha_{loss}L] - 1)$$
$$\times (1 + R \exp[h_{CD}(t) + h_{CH}(t)$$
$$+ h_{SHB}(t) - \alpha_{loss}L]) \frac{P_{in,RSOA}(t)}{E_{sat}} \quad (1)$$

$$\frac{dh_{CH}(t)}{dt} = -\frac{h_{CH}(t)}{\tau_{CH}} - \frac{\varepsilon_{CH}}{\tau_{CH}}(\exp[h_{CD}(t) + h_{CH}(t)$$
$$+ h_{SHB}(t) - \alpha_{loss}L] - 1)$$
$$\times (1 + R \exp[h_{CD}(t) + h_{CH}(t)$$
$$+ h_{SHB}(t) - \alpha_{loss}L]) P_{in,RSOA}(t) \quad (2)$$

$$\frac{dh_{SHB}(t)}{dt} = -\frac{h_{SHB}(t)}{\tau_{SHB}} - \frac{\varepsilon_{SHB}}{\tau_{SHB}}(\exp[h_{CD}(t) + h_{CH}(t)$$
$$+ h_{SHB}(t) - \alpha_{loss}L] - 1)$$
$$\times (1 + R \exp[h_{CD}(t) + h_{CH}(t)$$
$$+ h_{SHB}(t) - \alpha_{loss}L])$$
$$\times P_{in,RSOA}(t) - \frac{dh_{CD}(t)}{dt} - \frac{dh_{CH}(t)}{dt} \quad (3)$$

where functions 'h' represents the RSOA's gain integrated over its length due to the dynamic processes of the CD (h_{CD}), CH (h_{CH}), and SHB (h_{SHB}). $G_0 = \exp[2h_0]$ [16], where G_0 is the unsaturated power gain and the multiplicative factor of '2' due to the double pass of the input signal propagating in the RSOAs active region, while $G_0 = \exp[h_0]$ is considered for the conventional SOAs [12,13,24]. R is the rear-facet reflectivity, α_{loss} is the internal loss coefficient, and L is the length of the RSOA active region. $E_{sat} = P_{sat} \tau_C$ is the saturation energy, where P_{sat} is the saturation power and τ_C is the carrier lifetime. $P_{in,RSOA}(t)$ is the time-dependent input pulse power injected into each RSOA. τ_{CH} and τ_{SHB} are the temperature relaxation rate and carrier-carrier scattering rate, respectively. ϵ_{CH} and ϵ_{SHB} are the nonlinear gain suppression factors due to CH and SHB, respectively. The time-dependent gain equations for the conventional SOAs are presented in [24].

The total gain of each RSOA is then given by [27,28]:

$$G_{RSOA}(t) = R \, exp \, [2 \, (h_{CD}(t) + h_{CH}(t)$$
$$+ h_{SHB}(t) - \alpha_{loss}L)] \quad (4)$$

While the phase change incurred on the signal propagating through each RSOA is given by [27,28]:

$$\Phi_{RSOA}(t) = - (\alpha \, h_{CD}(t) + \alpha_{CH} \, h_{CH}(t)$$
$$+ \alpha_{SHB} \, h_{SHB}(t)) \quad (5)$$

where α is the traditional linewidth enhancement factor known as α-factor, α_{CH} is the linewidth enhancement factor due to CH, and α_{SHB} is the linewidth enhancement factor due to SHB. The contribution value of α_{SHB} should be zero because the SHB intraband dynamic process produces a nearly symmetrical spectral hole centred at the input signal wavelength [22,27,35].

In this study, the input optical pulses are assumed to be Gaussian-shaped whose power profile is described by [24,36]:

$$P_{A,B,Clk}(t) \equiv P_{in,RSOA}(t) = \sum_{n=1}^{N} a_{n(A,B,Clk)} \frac{2\sqrt{\ln[2]}E_0}{\sqrt{\pi} \tau_{FWHM}}$$
$$\times \exp \left[-\frac{4\ln[2](t - n \, T)^2}{\tau_{FWHM}^2} \right] \quad (6)$$

where $a_{n(A,B,Clk)}$ is the nth pulse, where $a_{n(A,B)}$ = '1' or '0' for the data streams A & B and a_{nClk} = '1' for the clock (Clk) signal inside a N = 2^n-1 [24] bit-long pseudorandom binary sequence (PRBS), where n is the equivalent PRBS length, which is assumed to equal 7 in this analysis [6,22,27,37]. E_0 is the pulse energy, τ_{FWHM} is the full-width at half maximum (FWHM) pulse width, and T is the bit period, which is the inverse of the data repetition rate measured in Gb/s (i.e. T = 1000/data rate). The format modulation of the input pulses used herein is a return-to-zero, which is widely used in optical systems owing to its attractive features [38–40].

To evaluate the performance quality of the considered Boolean functions, the QF metric is examined. This metric is defined as QF = $(P_1 - P_0)/(\sigma_1 + \sigma_0)$ [24,36], where $P_{1,0}$ are the mean peak powers of the '1' and '0' outputs and $\sigma_{1,0}$ are the corresponding standard deviations. The QF is a very sensitive metric used to provide the information of the optical signal to noise ratio in digital transmission. For acceptable performance, the QF value must be over six to ensure that keep the bit-error-rate (BER) at the minimum level $< 10^{-9}$ [24,27,28]. The BER is related to the QF in terms of BER = $(2\pi)^{-0.5} \exp[-0.5 QF^2]/QF$ [41,42]. The time-depended equations are prepared and run using the Adams numerical method Wolfram Mathematica®. For fair performance comparison, the same parameter values listed in Table 1 are used for both devices, except R = 0 and G_0 = $\exp[h_0]$ for the conventional SOAs, while R = 1 and G_0 = $\exp[2h_0]$ for the RSOA.

NOR logic gate at 120 Gb/s

The NOR logic gate is a logically inverted OR gate that gives '1' output only when both inputs are '0'. The schematic diagram and the corresponding truth table of the NOR logic gate using a dual-RSOAs-based scheme are illustrated in Figure 2.

AO NOR logic operation is based on cross-phase modulation (XPM) of two input signals in the (R)SOAs. To realize NOR operation, data streams A and B as pump signals are combined via a wavelength selective coupler (WSC) and launched into RSOA1 at port 1, while a clock (Clk) signal is inserted into RSOA2 from port 3. In parallel, a continuous wave (CW) beam as a probe is divided halves by a 3 dB optical coupler (OC) and injected into both RSOA1 and RSOA2 through the middle arm at port 2. Two WSCs are used in the forward direction to combine the CW beams with data streams and Clk signal travelling through RSOA1 and RSOA2, respectively, and split the outcomes from RSOAs to extract the CW beams that carry the NOR logical result. The data streams, A and B, and the Clk signal modulate the RSOAs' gain and

Table 1. Default numerical parameters.

Symbol	Definition	Value	Unit	Ref.
E_0	Pulse energy	0.2	pJ	[43]
τ_{FWHM}	Pulse width	1	ps	[13]
T	Bit period	8.33	ps	[27]
N	PRBS length	127	–	[22,27,37]
λ_A	Wavelength of signal A (NOR gate)	1549.2	nm	[6]
λ_B	Wavelength of signal B (NOR gate)	1535	nm	[6]
λ_{Clk}	Wavelength of Clk signal (NOR gate)	1555	nm	[6]
λ_{CW}	Wavelength of CW beam (NOR gate)	1550	nm	[6]
P_A	Power of signal A (NOR gate)	2	mW	[6]
P_B	Power of signal B (NOR gate)	2	mW	[6]
P_{Clk}	Power of Clk signal (NOR gate)	2	mW	[6]
P_{CW}	Power of CW beam (NOR gate)	1	mW	[6]
λ_A	Wavelength of signal A (XNOR gate)	1545	nm	[44]
λ_B	Wavelength of signal B (XNOR gate)	1550	nm	[44]
λ_{Clk}	Wavelength of Clk signal (XNOR gate)	1553.8	nm	[15]
λ_{CW}	Wavelength of CW beam (XNOR gate)	1545	nm	[15]
P_A	Power of signal A (XNOR gate)	1	mW	[45]
P_B	Power of signal B (XNOR gate)	1	mW	[45]
P_{Clk}	Power of Clk signal (XNOR gate)	2	mW	[15]
P_{CW}	Power of CW beam (XNOR gate)	2	mW	[45]
P_{sat}	Saturation power	10	mW	[22]
I	Injection current	100	mA	[13,27]
R	RSOA rear-facet reflectivity	1	–	[27]
L	Length of active region	0.4	mm	[9,27,46]
d	Thickness of active region	0.3	μm	[9,27]
α_{loss}	Internal loss coefficient	10	mm^{-1}	[27]
α	α-factor	6	–	[13]
α_{CH}	Linewidth enhancement factor due to CH	1	–	[13,27]
α_{SHB}	Linewidth enhancement factor due to SHB	0	–	[22,27,35]
τ_C	Carrier lifetime	100	ps	[13,27]
τ_{CH}	Temperature relaxation rate	0.3	ps	[24,13,27]
τ_{SHB}	Carrier-carrier scattering rate	0.1	ps	[24,13,27]
ϵ_{CH}	Nonlinear gain suppression factor due to CH	0.02	W^{-1}	[13,22,27]
ϵ_{SHB}	Nonlinear gain suppression factor due to SHB	0.02	W^{-1}	[13,22,27]
Γ	Optical confinement factor	0.15	–	[13,27]
G_0	Unsaturated power gain	30	–	[13,22,22]
B_0	Optical bandwidth	2	nm	[13,27]
υ	Optical frequency	1550	nm	[24]
N_{SP}	Spontaneous emission factor	2	–	[8,13,27]
T_{OP}	Operating temperature	20	°C	[13,24,27]

thereby the phase of the CW beam. The peak intensity of the pump signals and Clk signal are adjusted to be identical to give the same gain and phase modulation depth in each RSOA. The input optical signals propagate from the front facet through the active region and then reflected back by the HR rear facet to realize the output NOR gate at the output port of the optical circulator. When the combination of the high power signals A and B (10, 01, or 11) is launched into RSOA1 and a Clk signal (all 1's) is launched into RSOA2, both RSOAs get saturated, therefore, the modulated phases of the CW probe beam
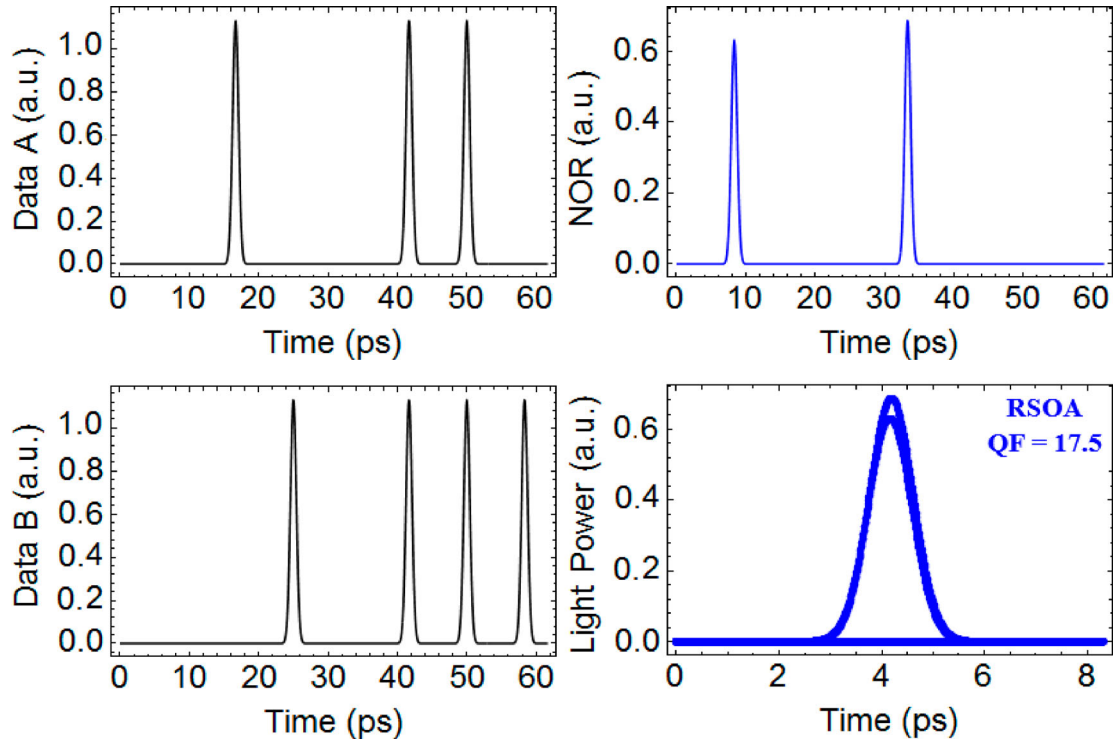
Figure 2. Schematic diagram and corresponding truth table of NOR gate using dual-RSOAs-based scheme. OC: 3 dB optical coupler. WSC: wavelength selective coupler.

travelling through RSOA1 and RSOA2 will be equal, which results in a logical '0' at the circulator output port due to destructive interference. When the combination of the low power signals A and B (00) is inserted into RSOA1, the Clk signal launched into RSOA2 will break the phase balance in both RSOAs, and hence '1' logic output is obtained at the circulator output port due to constructive interference. In this manner, the AO logic NOR gate is functionally realized between the binary signals A and B. The experimental setup for the NOR operation using SOA-based Mach–Zehnder interferometer (MZI) is presented in Ref. [6].

For the NOR operation, the total input powers inside the dual-RSOAs-based scheme are described by [12,24]:

$$P_{in,RSOA_1}(t) = P_A(t) + P_B(t) + 0.5P_{CW} \quad (7)$$

$$P_{in,RSOA_2}(t) = P_{Clk}(t) + 0.5P_{CW} \quad (8)$$

where the coefficient '0.5' refers to the coupling of the halving of the CW light via a 3 dB OC.

The NOR output power of the dual-RSOA-based scheme with the effect of the ASE (P_{ASE}) is then given by [9,12,24]:

$$P_{out,NOR}(t) = 0.25P_{CW}(G_{RSOA_1}(t) + G_{RSOA_2}(t)$$
$$- 2\sqrt{G_{RSOA_1}(t)G_{RSOA_2}(t)}$$
$$\cos[\Phi_{RSOA_1}(t) - \Phi_{RSOA_2}(t)]) + P_{ASE} \quad (9)$$

where $G_{RSOA1,2}(t)$ and $\Phi_{RSOA1,2}(t)$ are, respectively, the total gains and phase shifts experienced by the CW probe beam inside RSOA1 and RSOA2.

The main source of the noise in the (R)SOA is the ASE effect [24]. The spontaneous emission is generated during the amplification process and amplified during the active region. The optical amplifiers degrade the signal-to-noise ratio (SNR) of the amplified signal due to amplified spontaneous emission (ASE), which adds noise to the output signal. The ASE effect of the whole system is large even if each (R)SOA generates small ASE power because the ASEs are accumulated. The SNR is linked to the noise figure (NF) by NF = $(SNR)_{in}/(SNR)_{out}$ = 2 N_{SP} (G-1)/G, where N_{SP} is the spontaneous emission of the inversion factor [24]. In order to calculate the input and the output SNR, the spontaneous emission must be added [24]. The ASE power in the optical bandwidth (B_0) at a central frequency (v) is given by [24]:

$$P_{ASE} = N_{SP}(G_0 - 1)2\pi\hbar v B_0 \quad (10)$$

Using this equation, the noise effect on the gates' quality performance is numerically added to the equations of the gates' output powers numbered (11) for the NOR gate and (17) for the XNOR gate. There are many numerical models for calculating the noise value inside the amplifier. The model based on the spontaneous emission coupling factor is commonly used to calculate the ASE. The different shapes of the ASE spectrum at the two facets when the SOA is saturated [47]. A more direct numerical model to calculate the ASE is described in detail by Connelly [48]. The impact of the ASE can be experimentally measured by adding a few nm wide optical unmodulated signal to the input signals and then measuring the output QF as a function of the signal intensity and bandwidth.

Figures 3 and 4 show the numerical results of the NOR outcome and the corresponding eye diagram at 120 Gb/s using the dual-RSOAs-based scheme and SOAs-based MZI, respectively. The eye diagram is open and there are no pattern effects when using only RSOAs, as shown in Figure 3. Owing to the use of the RSOAs, the achieved QF is 17.5 compared to 4.7 when using the conventional bulk SOAs-based MZI at a data rate of 120 Gb/s.

Figure 5 shows the QF versus the rear-facet reflectivity (R) and the internal loss coefficient (α_{loss}) for the RSOA at 120 Gb/s for different bias currents, i.e. 50 and 100 mA. It can be seen from Figure 5(a) that the QF is rather increased with both R and I. This happens because the propagating input signal through the RSOA active region is amplified and reflected back by the RSOA rear facet to reach the RSOA front facet after making a double-pass to produce twice as much gain as in usual SOA. The RSOA feature can be used to obviate the need for extra optical fibre components and multiple optoelectronics optical devices. A different trend is observed in Figure 5(b) where the QF against α_{loss}. Although the QF is decreased as α_{loss} becomes more powerful, nevertheless this impact can be mitigated by raising the value of I at the expense of increased power consumption. Thus,

Figure 3. NOR numerical results at 120 Gb/s using dual-RSOAs-based scheme with 17.5 QF.
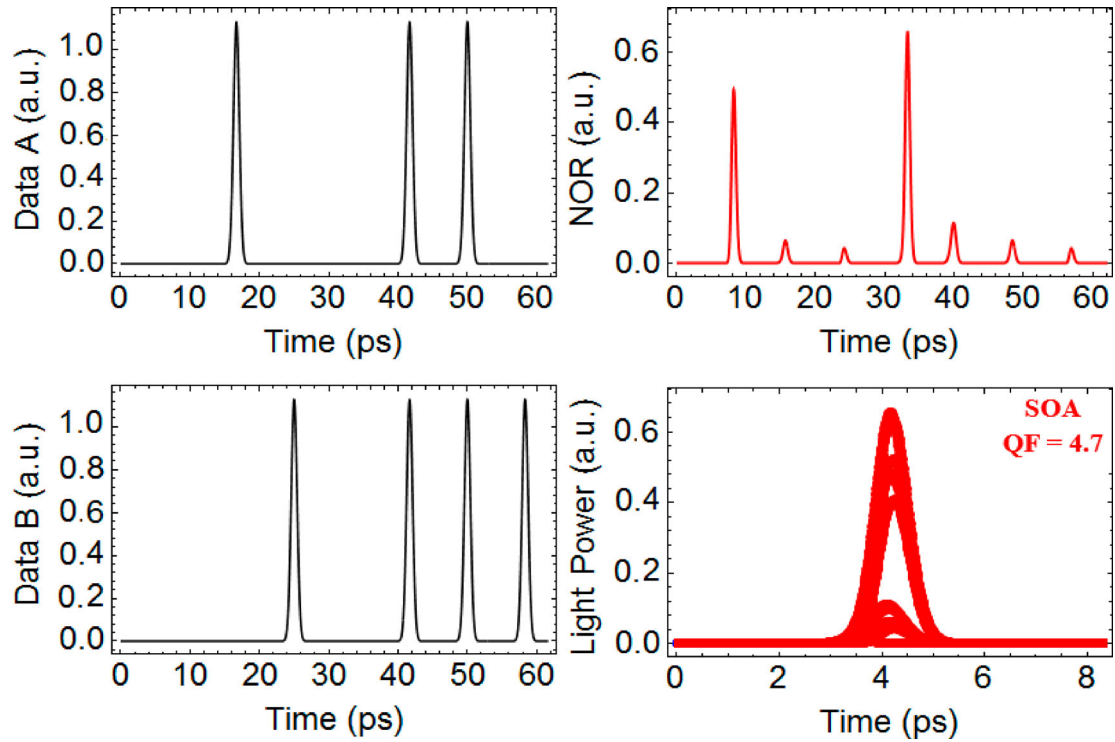

Figure 4. NOR numerical results at 120 Gb/s using conventional SOAs-based MZI with 4.7 QF.

100 mA injection current should be supplied to RSOAs to compensate α_{loss} of 10 mm^{-1} and achieve 17.5 QF.

It's recently well known that the SOAs have slow gain and phase recovery times, which limit their applications in higher data rates signal processing that does not exceed

$\sim$ 100 Gb/s. Although Figure 6(a) shows that the QF drops as the data rates become higher for both devices, its value ($\sim$ 7.37) remains acceptable, even up to 360 Gb/s when using RSOAs, while this is impossible when using conventional SOAs. Despite the operation of the NOR
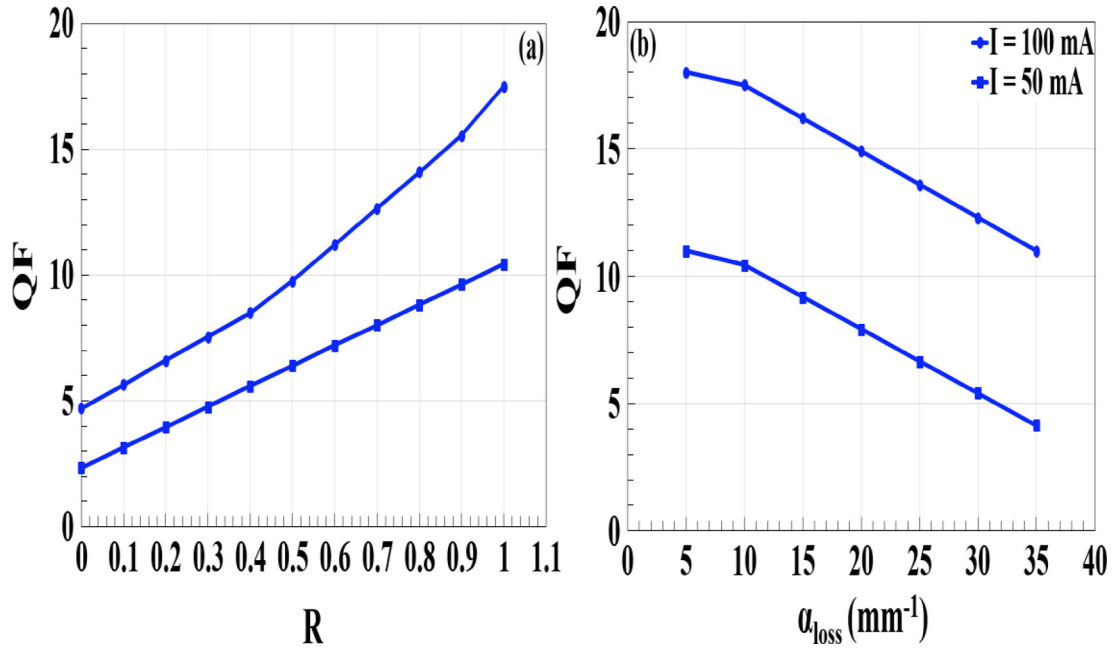
Figure 5. NOR QF versus RSOA (a) rear-facet reflectivity (R) and (b) internal loss coefficient (α_{loss}) at 120 Gb/s.
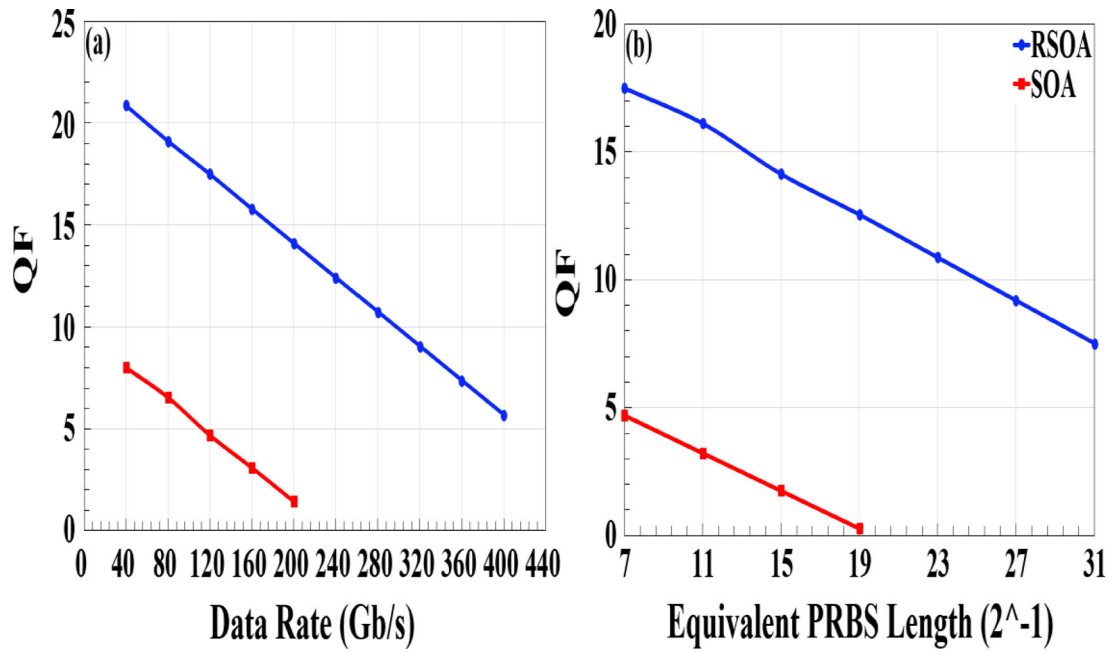
Figure 6. NOR QF versus (a) operating data rate and (b) equivalent PRBS length using dual-RSOAs-based scheme and conventional SOAs-based MZI at 120 Gb/s.

Boolean function is affected by higher equivalent PRBS lengths carried by each data as shown in Figure 6(b), the RSOAs scheme is tolerant to this effect and retains its acceptable QF value of ~ 7.52 at 31 equivalent PRBS length. These results confirm that the RSOAs scheme is potentially suitable for higher data rates and higher PRBS generations with better performance than conventional SOAs.

During the previous results, we considered the effects of the ASE noise and temperature to be fixed by considering that the two amplifiers are ideal (i.e. $N_{SP} = 2$) and operate at room temperature (i.e. $T_{OP} = 290$ K). However, their influence may affect the gates' performance. Thus, the effects of the ASE noise and T_{OP} on the QF for both schemes at different injection currents are depicted in Figure 7(a) and (b), respectively. The QF
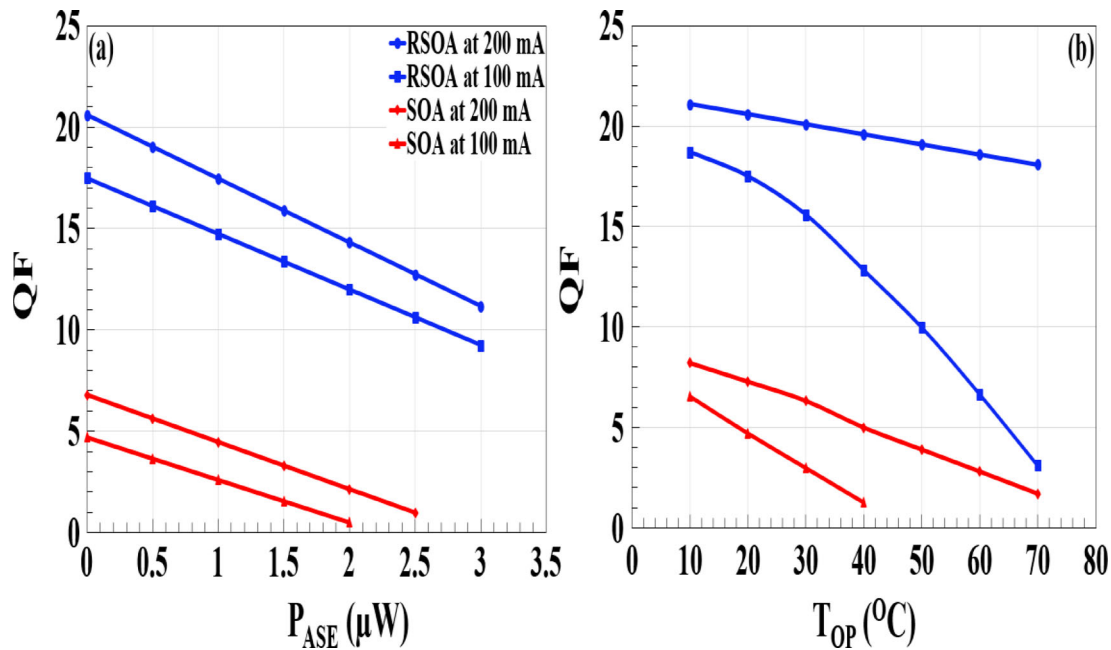
Figure 7. NOR QF versus (a) amplified spontaneous emission power (P_{ASE}) and (b) operating temperature (T_{OP}) using dual-RSOAs-based scheme and conventional SOAs-based MZI at 120 Gb/s for I = 100 and 200 mA.

is decreased with increase P_{ASE} for both amplifiers as shown in Figure 7(a) but its value remains acceptable when using RSOAs even at higher P_{ASE} values at the given currents. This happens because the RSOAs are operated at deep saturation where their gain dynamics are not critically affected by the ASE noise [49]. Similar behaviour is observed in Figure 7(b) where the QF is decreased as T_{OP} becomes higher for I = 200 mA and 100 mA. The effect of the operating temperature is considered in the numerical method using quasi-Fermi distribution equations presented in detail in chapter 4 of Connelly's book [50]. This is happened due to several reasons a) the electrons are distributed over a wider energy range at high T_{OP} and hence the number of electrons available for participating in the amplifier optical gain becomes fewer. b) The nonradiative recombination, which causes a reduction in QF, increases with T_{OP}. Moreover, the RSOA is packaged in a TO-can type, which is simple and important for the uncooled operation [24]. Thus, the QF using RSOA is still an acceptable value even at higher T_{OP}, while SOA must be operated at a low temperature for better performance [51]. Figure 7(a) indicates that the higher currents ≥ 200 mA must be employed to avoid the QF degradation generated by high T_{OP} especially in the RSOA case.

XNOR logic gate at 120 Gb/s

The XNOR logic gate is a logically inverted XOR gate that gives '1' output when only all inputs are '1' or '0'. The

schematic diagram and the corresponding truth table of the dual-RSOAs-based XNOR gate are illustrated in Figure 8.

The XOR gate is realized herein by a series combination of the XOR and INVERT operations [24]. Two steps are required to perform the XNOR gate, i.e. XOR operation as the first step and then the INVERT operation. For the XOR operation, two data signals A and B are separately inserted into RSOA1 and RSOA2 at port 1 and port 3 via WSCs, respectively, while a CW probe beam is split via 3 dB OC and then coupled into both RSOA1 and RSOA2 from the middle at port 2. The data streams A and B modulate the RSOAs' gain and thereby the phase of the CW probe beam via XPM, which provides better performance and higher power efficiency than a cross-gain modulation [52]. More specifically, when A = B = '0', the CW beam making a double-pass through RSOA1 and 2 does not acquire any phase shift, resulting in '0' logic output. However, when A = B = '1', the CW beam experiences the same phase shift inside both RSOA1 and 2, so they interfere destructively and result in '0' logic output. While A = '1' and B = '0', the CW beam travelling with signal A inside RSOA1 suffers through XPM a phase shift versus its copy propagating inside RSOA2, thus the CW beam interferes constructively, which results in '1' output. The same outcome was obtained when A = '0' and B = '1'. In this manner, the XOR gate is executed between binary signals A and B at the circulator output. The XOR operation has been experimentally demonstrated using SOAs-MZI as in [44]. Then to realize the
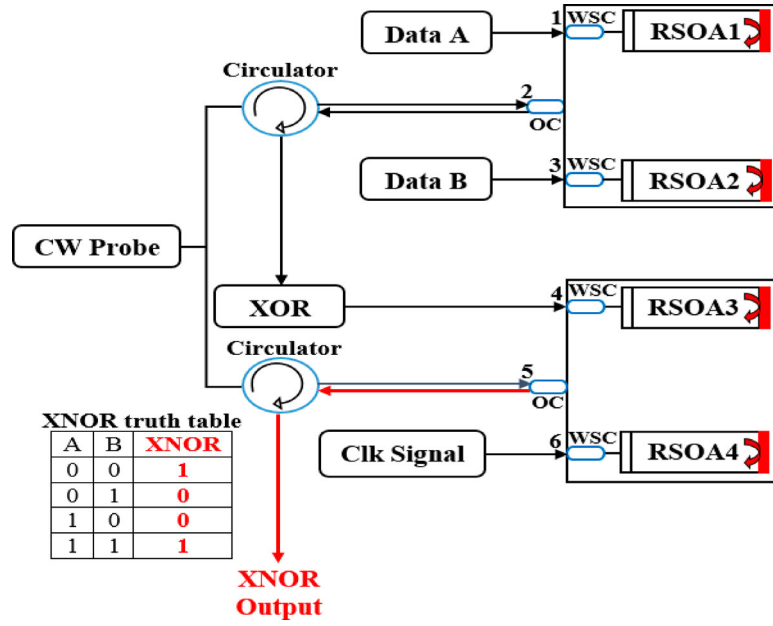
Figure 8. Schematic diagram and corresponding truth table of dual-RSOAs-based XNOR gate. OC: 3 dB optical coupler. WSC: wavelength selective coupler.

INVERT operation, the XOR output is launched via a WSC into RSOA3 at port 4, while a Clk signal is launched into RSOA4 at port 6 and a CW is a parallel sent from port 5 as shown in Figure 8. In this manner, the AO XNOR output gate is achieved between binary contents of input data streams A and B.

The input powers inside RSOA1 and RSOA2 for the XOR operation using the dual-RSOAs-based scheme are described by [13,45]:

$$P_{in,RSOA_1}(t) = P_A(t) + 0.5P_{CW} \tag{11}$$

$$P_{in,RSOA_2}(t) = P_B(t) + 0.5P_{CW} \tag{12}$$

The XOR output power of the proposed scheme with the ASE effect is given by the following basic interferometric equation [24,45]:

$$P_{out,XOR}(t) = 0.25P_{CW}(G_{RSOA_1}(t) + G_{RSOA_2}(t)$$
$$- 2\sqrt{G_{RSOA_1}(t)G_{RSOA_2}(t)}$$
$$\cos[\Phi_{RSOA_1}(t) - \Phi_{RSOA_2}(t)]) + P_{ASE} \tag{13}$$

While the total input powers inside RSOA3 and RSOA4 for the INVERT operation are described by [20,22]:

$$P_{in,RSOA_3}(t) = P_{out,XOR}(t) + 0.5P_{CW} \tag{14}$$

$$P_{in,RSOA_4}(t) = P_{Clk}(t) + 0.5P_{CW} \tag{15}$$

Then, the XNOR output power with the ASE effect is given by [20,36]:

$$P_{out,XNOR}(t) = 0.25P_{CW}(G_{RSOA_3}(t) + G_{RSOA_4}(t)$$

$$- 2\sqrt{G_{RSOA_3}(t)G_{RSOA_4}(t)}$$
$$\cos[\Phi_{RSOA_3}(t) - \Phi_{RSOA_4}(t)]) + P_{ASE} \tag{16}$$

Figures 9 and 10 show the numerical results for the XNOR logic function at 120 Gb/s using the dual-RSOAs-based scheme and SOAs-based MZIs, respectively. It can be seen from Figure 10 that there are no pattern effects and the eye diagram is clear with 19.3 QF when using a dual-RSOAs-based scheme, while the QF of SOAs-MZIs is an unacceptable value of 5.4.

The following results obtained for the XNOR gate have been numerically calculated in the same way as described for the NOR logic gate.

Figure 11 shows the XNOR QF as a function of the rear-facet reflectivity (R) and the internal loss coefficient (α_{loss}) of the RSOA at 120 Gb/s for I = 50 and 100 mA.

The dependence of the XNOR QF on the operating data rate and the equivalent PRBS length using both schemes at 120 Gb/s is shown in Figure 12. This figure confirms that the XNOR can be implemented using RSOAs with higher QF than SOAs even at higher data rates and longer PRBS.

The QF dependence on the ASE power (P_{ASE}) and operating temperature (T_{OP}) for the XNOR operation at 120 Gb/s using both schemes has been calculated for different injection currents, as shown in Figure 13(a) and (b), respectively. The ASE effect on the XNOR performance is due to the contribution both from the XOR and INVERT operations. The ASE power is numerically added to the XNOR output power given by equation
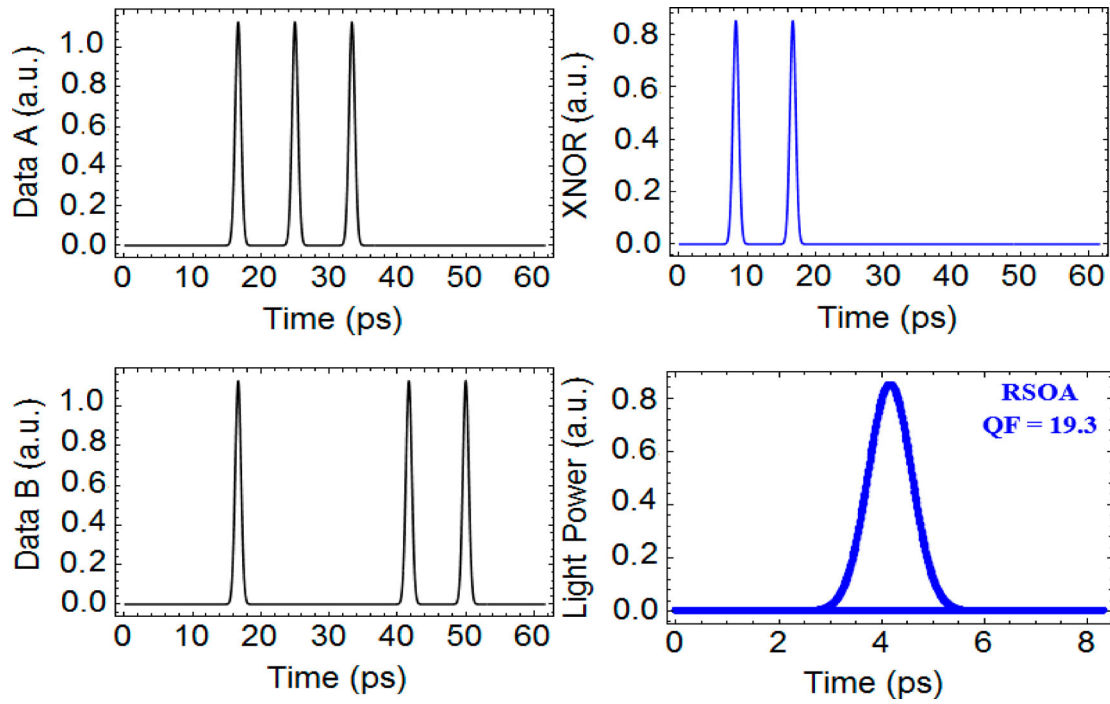
Figure 9. XNOR numerical results at 120 Gb/s using dual-RSOAs-based scheme with 19.3 QF.
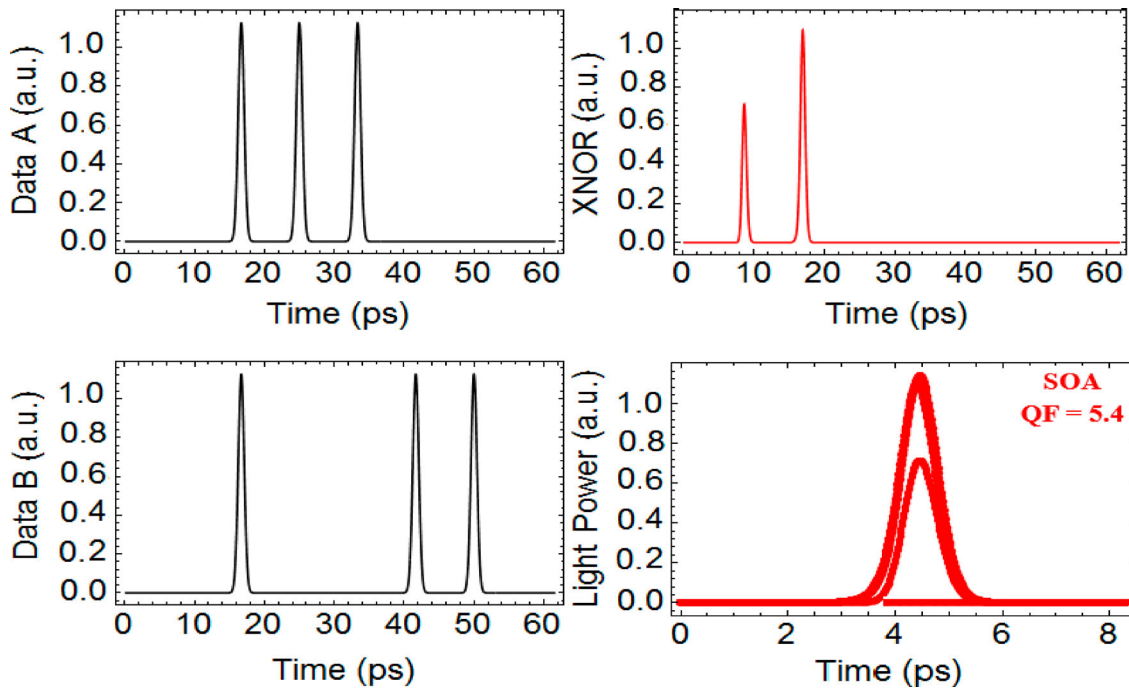

Figure 10. XNOR numerical results at 120 Gb/s using conventional SOAs-based MZIs with 5.4 QF.

(16) using equation (10) in the same way as described in the NOR operation. The QF using RSOAs remains acceptable, even at higher ASE power, while this does not happen when using SOAs, as shown in Figure 13(a). On the other hand, higher currents can be used to avoid degradation in the QF due to higher T_{OP} as shown in Figure 13(b). From these results, we believe that the

RSOAs can operate with more acceptable performance at higher noise and higher temperatures.

2. Conclusions

In this study, the ultrafast performance of all-optical (AO) NOR and XNOR gates using dual-reflective
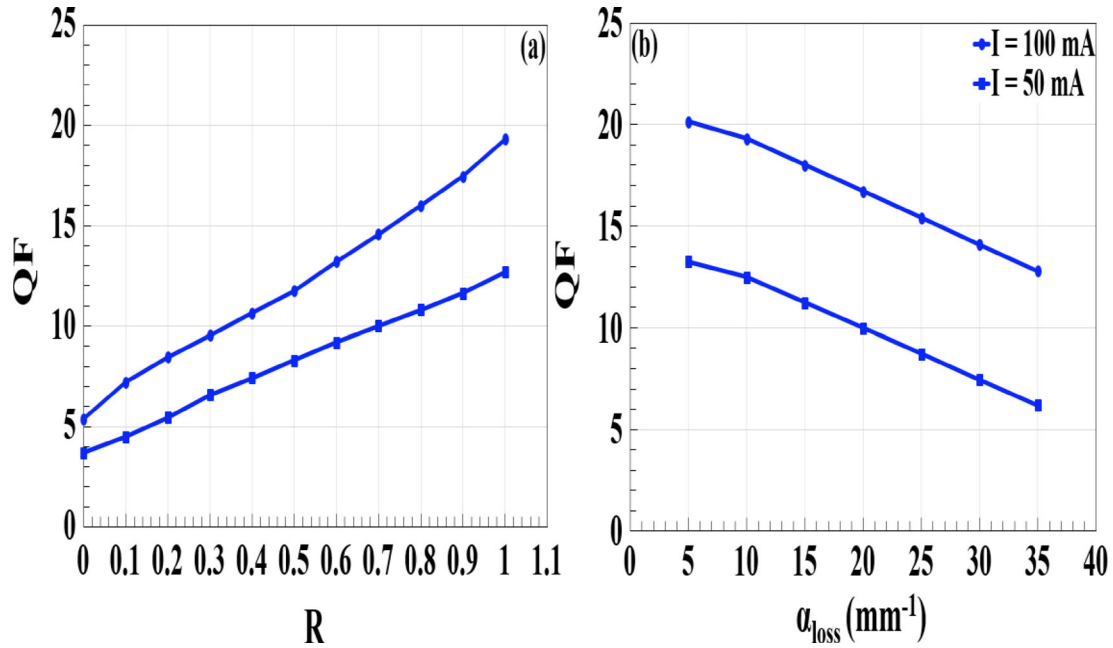
Figure 11. XNOR QF versus RSOA (a) rear-facet reflectivity (R) and (b) internal loss coefficient (α_{loss}) at 120 Gb/s.
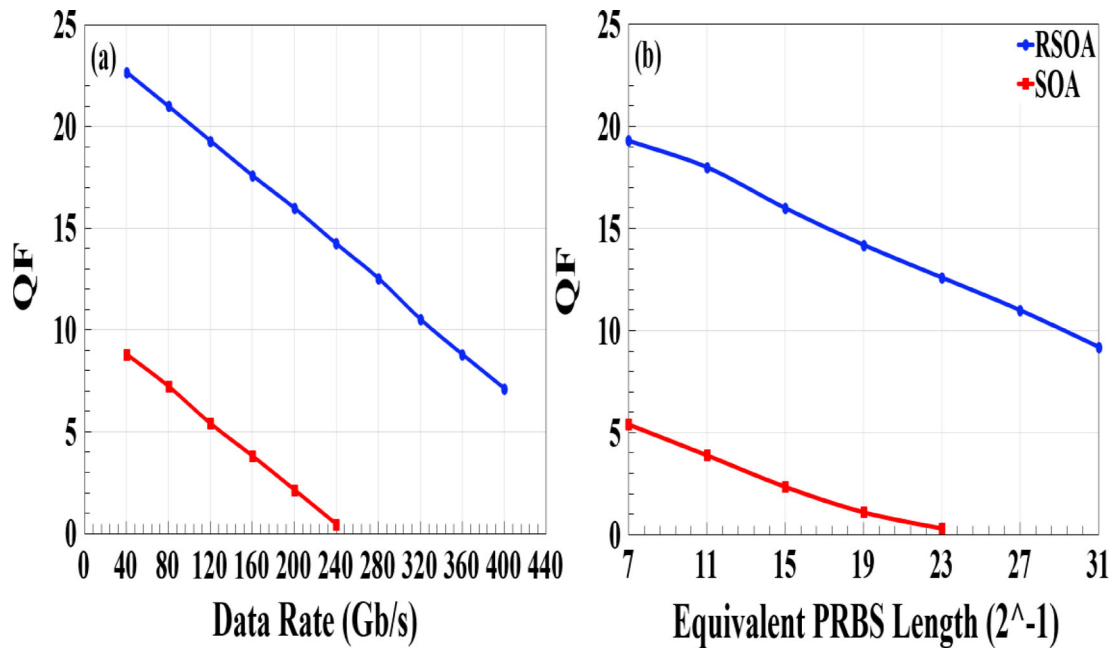
Figure 12. XNOR QF versus (a) operating data rate and (b) equivalent PRBS length using dual-RSOAs-based scheme and conventional SOAs-based MZIs at 120 Gb/s.

semiconductor optical amplifiers (RSOAs)-based scheme has been successfully numerical investigated at a data rate of 120 Gb/s. A fair comparison between RSOAs and conventional bulk SOAs was made by examining the dependence of the quality factor (QF) on the key operational parameters such as rear-facet reflectivity (R), internal loss coefficient, operating data rate, and pseudorandom binary sequence (PRBS), including the effects of the amplified spontaneous emission and the operating temperature for more realistic calculations. Overall, the outcomes confirm that the considered Boolean functions, NOR and XNOR, can be executed using RSOAs at 120 Gb/s with higher QF than if SOAs were used instead. We believe that the proposed scheme will play a main role in constriction high-speed logic circuits.
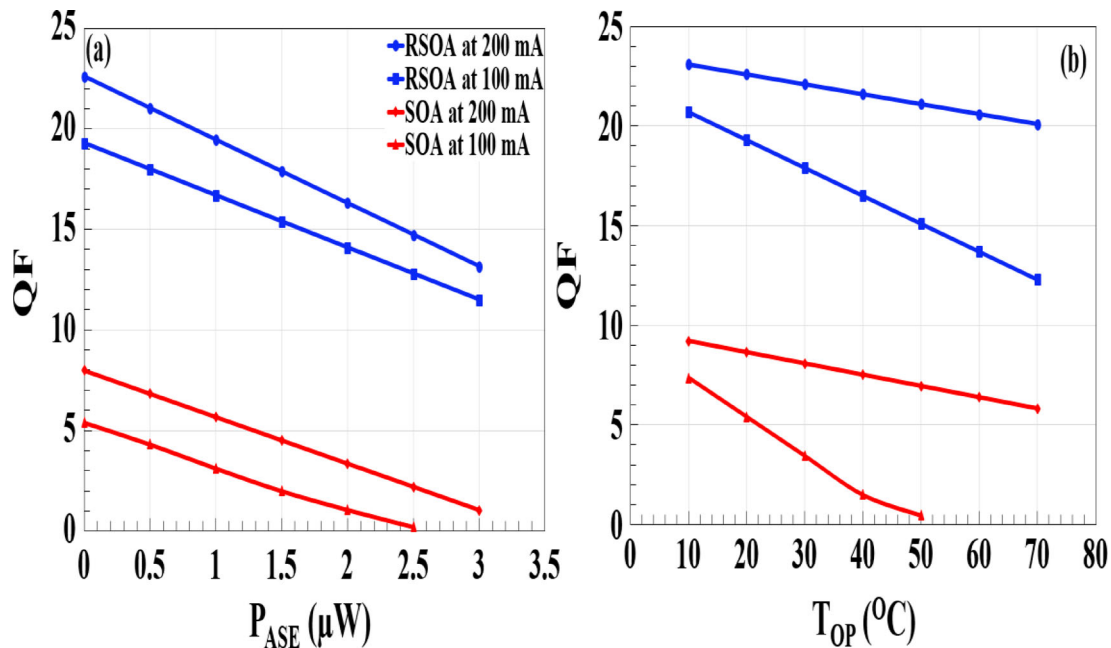
Figure 13. XNOR QF versus (a) amplified spontaneous emission power (P_{ASE}) and (b) operating temperature (T_{OP}) using dual-RSOAs-based scheme and conventional SOAs-based MZIs at 120 Gb/s for I = 100 and 200 mA.

Disclosure statement

No potential conflict of interest was reported by the author(s).

ORCID

Amer Kotb http://orcid.org/0000-0002-3776-822X
Chunlei Guo http://orcid.org/0000-0001-8525-6301

References

[1] Byun YT, Kim JH, Jhon YM, et al. High-speed all-optical NOR gate using semiconductor optical amplifier. Conference Lasers and Electro-Optics Europe; 2003.

[2] Sharaiha A, Topomondzo J, Morel P. All-optical logic AND-NOR gates with three inputs based on cross-gain modulation in a semiconductor optical amplifier. Opt Commun. 2006;265:322–325.

[3] Kim JY, Kang JM, Kim TY, et al. All-optical multiple logic gates with XOR, NOR, OR and NAND function using parallel SOA-MZI structures: theory and experiment. J Lightwave Technol. 2006;24:3392–3399.

[4] Kim JY, Kang JM, Kim TY, et al. 10 Gbits all-optical composite logic gates with XOR, NOR, OR and NAND functions using SOA-MZI structures. Electron Lett. 2006;42:303–307.

[5] Xu J, Zhang X, Liu D, et al. Ultrafast all-optical NOR gate based on semiconductor optical amplifier and fiber delay interferometer. Opt Express. 2006;14:10708–10714.

[6] Sun H, Chen Z, Ma S, et al. All-optical logic NOR gate using SOA based Mach-Zehnder interferometer. Proc SPIE. 2007;6775:67750F.

[7] Dong J, Zhang X, Xu J, et al. 40 Gb/s all-optical logic NOR and OR gates using a semiconductor optical amplifier: experimental demonstration and theoretical analysis. Opt Commun. 2008;281:1710–1715.

[8] Kotb A, Ma S, Chen Z, et al. Effect of amplified spontaneous emission on semiconductor optical amplifier based all-optical logic. Opt Commun. 2011;284:5798–5803.

[9] Kotb A. Simulation of all-optical logic NOR gate based on two-photon absorption with semiconductor optical amplifier-assisted Mach-Zehnder interferometer with the effect of amplified spontaneous emission. Korean Phys Soc. 2015;66:1593–1598.

[10] El-Saeed EM, Abd El-Aziz A, Fayed HA, et al. Optical logic gates based on semiconductor optical amplifier Mach–zehnder interferometer: design and simulation. Opt Eng. 2016;55:025104.

[11] Chen X, Huo L, Zhao Z, et al. Study on 100-Gb/s reconfigurable all-optical logic gates using a single semiconductor optical amplifier. Opt Express. 2016;24:30245–30253.

[12] Kotb A. Theoretical analysis of soliton NOR gate with semiconductor optical amplifier-assisted Mach-Zehnder interferometer. Opt Quantum Electron. 2017;49:1–12.

[13] Kotb A, Zoiros KE, Guo C. All-optical XOR, NOR, and NAND logic functions with parallel semiconductor optical amplifier-based Mach-Zehnder interferometer modules. Opt Laser Technol. 2018;108:426–433.

[14] Han B, Liu Y. All-optical reconfigurable non-inverted logic gates with a single semiconductor optical amplifier. AIP Adv. 2019;9:015007.

[15] Lee S, Park J, Lee K, et al. All-optical exclusive NOR logic gate using Mach-Zehnder interferometer. Jpn J Appl Phys. 2002;41:1155–1157.

[16] Kim JH, Kim YI, Byun YT, et al. All-optical logic gates using semiconductor optical-amplifier-based devices and their applications. Korean Phys Soc. 2004;45:1158–1161.

[17] Kang I, Rasras M, Buhl L, et al. All-optical XOR and XNOR operations at 86.4 Gb/s using a pair of semiconductor optical amplifier Mach-Zehnder interferometers. Opt Express. 2009;17:9062–19065.

[18] Singh S L. Ultrahigh-speed optical signal processing logic based on an SOA-MZI. IEEE J Sel Top Quantum Electron. 2012;18:970–975.

[19] Kotb A, Maeda J. All-optical logic NXOR based on semiconductor optical amplifiers with the effect of amplified spontaneous emission. Optoelectron Lett. 2012;8:437–440.

[20] Kotb A. Performance of all-optical XNOR gate based on two-photon absorption in semiconductor optical amplifiers. Adv. Opt Technol. 2014;2014:754713.

[21] Xi L, Jie J, Haitao L, et al. Study of all-optical logic XNOR gate based on XGM in linear optical amplifier. J Mod Opt. 2017;64:59–66.

[22] Kotb A. Computational analysis of soliton all-optical logic NAND and XNOR gates using semiconductor optical amplifiers. Opt Quantum Electron. 2017;49:1–17.

[23] Dúill S Ó, Marazzi L, Parolari P, et al. Efficient modulation cancellation using reflective SOAs. Opt Express. 2012;20:587–594.

[24] Dutta NK, Wang Q. Semiconductor optical amplifiers. 2nd ed. Singapore: World Scientific Publishing Company; 2013.

[25] Bogoni A, Potì L, Ghelfi P, et al. OTDM-based optical communications networks at 160 Gbit/s and beyond. Opt Fiber Technol. 2007;13:1–12.

[26] Mulvad HCH, Galili M, Oxenløwe LK, et al. Demonstration of 5.1 Tbit/s data capacity on a single-wavelength channel. Opt Express. 2010;18:1438–1443.

[27] Kotb A, Zoiros KE, Guo C. Performance investigation of 120 Gb/s all-optical logic XOR gate using dual-reflective semiconductor optical amplifier-based scheme. J Comp Electron. 2018;17:1640–1649.

[28] Kotb A, Guo C. 120 Gb/s all-optical NAND logic gate using reflective semiconductor optical amplifiers. J Mod Opt. 2020;67:1138–1144.

[29] Dúill S Ó, Barry LP. Improved reduced models for single-pass and reflective semiconductor optical amplifiers. Opt Commun. 2015;334:170–173.

[30] Antonelli C, Mecozzi A. Reduced model for the nonlinear response of reflective semiconductor optical amplifiers. IEEE Photon Technol Lett. 2013;25:2243–2246.

[31] Cassioli D, Scotti S, Mecozzi A. A time-domain computer simulator of the nonlinear response of semiconductor optical amplifiers. IEEE J Quantum Electron. 2000;36:1072–1080.

[32] Antonelli C, Mecozzi A, Hu Z, et al. Analytic study of the modulation response of reflective semiconductor optical amplifiers. J Lightwave Technol. 2015;33:4367–4376.

[33] Connelly MJ. Reflective semiconductor optical amplifier pulse propagation model. IEEE Photon Technol Lett. 2012;24:95–97.

[34] Sengupta I, Barman AD. Analysis of optical re-modulation by multistage modeling of RSOA. Optik. 2014;125:3393–3400.

[35] Schares L, Schubert C, Schmidt C, et al. Phase dynamics of semiconductor optical amplifiers at 10 to 40 GHz. IEEE J Quantum Electron. 2003;39:1394–1408.

[36] Kotb A. All-optical logic gates using semiconductor optical amplifier. Saarbrucken: Lambert Academic Publishing; 2012.

[37] Kotb A, Zoiros KE. Performance analysis of all-optical XOR gate with photonic crystal semiconductor optical amplifier-assisted Mach–zehnder interferometer at 160 Gb/s. Opt Commun. 2017;402:511–517.

[38] Breuer D, Petermann K. Comparison of NRZ- and RZ-modulation format for 40-Gb/s TDM standard-fiber systems. IEEE Photon Technol Lett. 1997;9:398–400.

[39] Kawanishi S. Ultrahigh-speed optical time-division-multiplexed transmission technology based on optical signal processing. IEEE J Quantum Electron. 1998;34:2064–2079.

[40] Zhu G, Wang Q, Chen H, et al. High-quality optical pulse train generation at 80 Gb/s using a modified regenerative-type mode-locked fiber laser. IEEE J Quantum Electron. 2004;40:721–725.

[41] Zhang X, Dutta NK. Effects of two-photon absorption on all-optical logic operation based on quantum-dot semiconductor optical amplifiers. J Mod Opt. 2018;65:166–173.

[42] Thapa S, Zhang X, Dutta NK. Effects of two-photon absorption on pseudo-random bit sequence operating at high speed. J Mod Opt. 2019;66:100–108.

[43] Kotb A, Guo C. All-optical OR and NOR gates using quantum-dot semiconductor optical amplifiers-assisted turbo-switched Mach-Zehnder interferometer and serially delayed interferometer at 1 Tb/s. Optik. 2020;218:164879.

[44] Wang Q, Zhu G, Chen H, et al. Study of all-optical XOR using Mach-Zehnder interferometer and differential scheme. IEEE J Quantum Electron. 2004;40:703–710.

[45] Kotb A, Zoiros KE, Guo C. 320 Gb/s all-optical XOR gate using semiconductor optical amplifier Mach-Zehnder interferometer and delayed interferometer. Photon Netw Commun. 2019;38:177–184.

[46] Li Q, Ma S, Hu H, et al. All-optical latches based on two-photon absorption in semiconductor optical amplifiers. J Opt Soc Am B. 2012;29:603–2609.

[47] Talli G, Adams MJ. Amplified spontaneous emission in semiconductor optical amplifiers: Modelling and experiments. Opt Commun. 2003;218:161–166.

[48] Connelly MJ. Wideband semiconductor optical amplifier steady-state numerical model. IEEE J Quantum Electron. 2001;37:439–447.

[49] Wei JL, Yang XL, Giddings RP, et al. Colourless adaptively modulated optical OFDM transmitterd using SOAs as intensity modulators. Opt Express. 2009;17:9012–9027.

[50] Connelly MJ. Semiconductor optical amplifiers. New York: Kluwer Academic Publisher; 2004.

[51] Kumar Y, Shenoy MR. Temperature dependence of operational characteristics of semiconductor optical amplifier. 12th International Conference on Fiber Optics and Photonics 2014 2014;M4A.64:1–3.

[52] Durhuus T, Mikkelsen B, Joergensen C, et al. All-optical wavelength conversion by semiconductor optical amplifiers. J Lightwave Technol. 1996;14:942–954.